Upper Cretaceous-Cenozoic uplifts and tectonics within a Precambrian shield - insight from the Hoggar (Algeria) local sedimentary cover

Mohamed E M Derder, Said Maouche, Yves Missenard, Bernard Henry, Mohamed Amenna, Aziouz Ouabadi, Boualem Bayou, Rafik Bestandji, Djouher Kettouche, Hamid Haddoum

Upper Cretaceous - Cenozoic uplifts and tectonics within a Precambrian shield – Insight from the Hoggar (Algeria) local sedimentary cover.

Mohamed E.M. Derder[1*], Said Maouche[1], Yves Missenard[2], Bernard Henry[3], Mohamed Amenna[1], Aziouz Ouabadi†[4], Boualem Bayou†[1], Rafik Bestandji[1], Djouher Kettouche[2+] and Hamid Haddoum[4]

[1] *CRAAG, B.P. 63, Bouzaréah 16340 Alger, Algeria.*

[2] *GEOPS, UMR8148, Université Paris-Saclay, 91405 Orsay, France.*

[3] *Univ. Paris Cité, Institut de Physique du Globe de Paris (IPGP), Sorbonne Paris Cité, and UMR 7154 CNRS, 1 rue Jussieu, 75238 cedex 05, France, France.* Orcid: 0000-0002-2576-5144

[4] *Laboratoire "Géodynamique, Géologie de l'Ingénieur et Planétologie", FSTGAT / USTHB, BP 32, El-Alia Bab Ezzouar, 16111 Alger, Algeria.*

+ Now at Department of Geology, FSTGAT / USTHB, BP 32, El-Alia Bab Ezzouar, 16111 Alger, Algeria.

† Deceased.

* Corresponding author *Tel : +213 23 18 90 98 ; Fax : +213 23 18 91 01* m.e.m.derder@gmail.com; orcid:0000-0003-0212-7294.

Email addresses: m.e.m.derder@gmail.com (M.E.M. Derder); said.maouche@gmail.com (S. Maouche); yves.missenard@universite-paris-saclay.fr (Y. Missenard); henry@ipgp.fr (B. Henry); mohamed20_dz@yahoo.fr (M. Amenna); bestandjirafik@gmail.com (R. Bestandji); jouher.kettouche@gmail.com (D. Kettouche); haddoum_hamid@yahoo.fr (H. Haddoum)

Abstract

In order to better constrain the Mesozoic-Cenozoic evolution of the Precambrian Hoggar shield, a paleomagnetic study, combined with detailed fieldwork, was carried out to date its detrital local cover, the Serouenout Formation. Thermal demagnetization yields, only in a few samples, the Characteristic Remanent Magnetization carried by hematite. Post-tilting remagnetization was obtained in sites located along a fault affected by intense fluids circulation. The paleomagnetic directions recorded at seven widespread other sites are on the contrary associated with a positive fold test. It provides a relatively well-defined paleomagnetic pole (A_{95} = 4.1°), sufficient to estimate the age of the Serouenout Formation. The comparison of this pole with the reference curve of Africa suggests two possible age windows, Triassic and Upper Cretaceous-Lower Paleocene, while the

discovery in the uppermost levels of the Serouenout Formation of a fern-rich level with *Weichselia reticulata* (Bathonian to Cenomanian; Blanco-Moreno et al., 2018) imposes a deposition during the Cenomanian. The presence of a detrital formation at least 350 m thick, with a basal conglomerate containing large pebbles implies the existence, during this time period, of a tectonic event that generated differential uplift. In addition, structural observations indicate that the Serouenout Formation recorded later brittle tectonics, dominated by a network of vertical N-S dextral faults. The horizontal displacement generated by one well-developed fault has been estimated to be at least 1 km. This activity is related to the known Alpine reactivations of the N-S Pan-African mega-structures, which are still at the origin of the current intraplate seismicity.

Keywords: Paleomagnetism, Paleobotanic, Cenomanian, Brittle tectonics, Uplift, Alpine reactivation, Hoggar.

Introduction

The intraplate Hoggar shield in Sahara mainly corresponds to a 1000 km large basement swell with 1000 to 1500 m average altitudes. It is made of several "terranes" amalgamated through the reactivation of large mainly N-S shear zones during the Pan-African orogeny (Black et al. 1994). The new synthetic geological map of the Hoggar shield (Liégeois 2019) shows that, in the northeastern part of the Hoggar, the juvenile allochthonous Serouenout terrane is thrust sheets resting over a Paleoproterozoic (Orosirian - Baziz et al. 2005) basement, the Afara terrane. The Serouenout and Afara terranes are separated to the west from the LATEA metacraton (Liégeois et al. 2003, Ouzegane et al. 2023) by the N-S Ounane major shear zone (e.g., Nouar et al 2021). Afara, Assodé-Issalane and Tazat terranes (separated by “secondary” major shear zones) constitute the Orosirian Stripe (Liégeois 2019), bounded to the East by the N-S Raghane major shear zone. The preservation of the Serouenout terrane is probably due to a less important uplift of the Afara terrane within this area, being then a depression at that time. The sediments (Serouenout Formation), considered in this study, were deposited on this Afara terrane and preserved in a depression situated just to the north of the Serouenout terrane. This area was locally covered by Cenozoic volcanic flows (Aït-Hamou et al. 2000; Liégeois et al. 2005).

The Serouenout formation (Fig. 1) consists of poorly dated red clay-sandstones (Lower Cretaceous to Lower Cenozoic in age, Bordet, 1955). The facies homogeneity (often with cross-bedding stratification) within all the basin suggest deposition in a single large river-lake system. The formation, reaching 350 m thickness, was

affected by slight deformation after deposition (Bordet, 1955). Knowing the age of this formation, which characterizes a local episode of subsidence, is key to understanding the evolution of the Hoggar massif.

On another hand, the current elevation of the Hoggar is a consequence of an uplift whose origin remains debated (e.g., Lesquer et al. 1988; Aït Hamou and Dautria, 1994, Beccaluva et al. 2007; Liégeois et al. 2005) but large-scale vertical processes can be assessed (Rougier et al., 2013).

A paleomagnetic study (Derder et al. 2023), associated with a detailed field work, was therefore attempted to better specify the Serouenout Formation age and the Mesozoic-Cenozoic structural evolution of the Precambrian Hoggar shield.

Cretaceous-Cenozoic structural events in the Hoggar area

Several regional-scale rift basins (Tafassasset, Ténéré, Tefidet) developed during the Late Mesozoic east and south of the Hoggar (e.g., Louis and Rechenmann, 1966; Dautria and Lesquer, 1989, Zhou et al. 2017). On the western and northern Hoggar borders, a folding event occurred around the Upper Jurassic – Lower Cretaceous (Smith et al. 2006; Derder et al. 2009). The Lower Cretaceous Austrian tectonic phase is well known in the sedimentary basins (e.g., Oued Mya) north of the Hoggar (e.g., Boudjema and Tremolières, 1987; Maurin and Guiraud, 1993; Guiraud et al. 2005; Craig et al. 2008). Another major tectonic event in this area was the Hoggar uplift. Faure (1985), using sedimentological criteria, stipulated that this uplift would have started during the Cretaceous. Rougier et al. (2013) showed, using thermochronological data, that the Hoggar was buried between 95 Ma and 40 Ma and that the main uplift occurred between 40 Ma and 35 Ma. For these authors "The outcrops of Cretaceous sedimentary remnants in the northeastern part of the swell are consistent with Upper Cretaceous – Eocene burying under a 1- to 3-km-thick sedimentary cover. Whether this cover was extended to the whole Tuareg Shield is not yet documented. If the depositional area was confined to the Aïr and northeastern Hoggar, Cretaceous Ténére troughs could have crossed the Hoggar on its northeastern part. On the other hand, extension of the cover over the whole shield would evidence that a large intraplate sag basin developed."

Field data

Lithology

The Paleozoic cover of the Saharan platform (outcropping far to the east and to the north of the Hoggar) was eroded within the Hoggar before the deposition of Serouenout sandstones. The Serouenout sediments rest unconformably on an Eburnean basement.

From a lithologic point of view, these fluvial and lacustrine sediments include various facies, often characterized by cross-bedding. Figure 2 shows a synthetic stratigraphic column based on the most complete section at Tin Adakitine (Fig. 1). From the bottom to the top:

1) Basal conglomerate with large, often rounded, pebbles (up to several tens of kilogram and sometimes broken – Bordet, 1955, Fig. 3) and coarse arkosic sandstones (pinkish to reddish color).

2) Light pink sandstones rich in quartz grains.

3) Muddy sandstone levels (reddish to purplish) characterized by cross-bedding.

4) Alternate mudstone and sandstones.

5) Calcareous sandstones (probably silicified lacustrine limestones).

The total thickness of this almost complete section (only the basal conglomerate is missing), located on a basin border (Tin Adakitine, Fig. 1a), is 150 m while the Serouenout Formation thickness reaches mostly 350 m (Bordet, 1955). The SW-NE cross-section (Fig. 4) of the basin also shows that the base of the Serouenout Formation altitude is between 1100 and 1700 m high (Bordet, 1955; Rougier, 2012).

This sedimentary formation is covered by trachytic and basaltic lava (35 to 24 Ma) related to the well exposed volcanism in the Serouenout district and in the Atakor region to the west (Bordet, 1955; Aït Hamou, 2000; Aït Hamou et al. 2000; Azzouni-Sekkal et al. 2007; Benhallou et al. 2019). Locally, the lava settled over an irregular topography (e.g., cliffs of sedimentary levels), highlighting erosion prior to the volcanism (Bordet, 1955).

New structural observations

For Bordet (1955), the sedimentary formations of the Serouenout basin have been affected by weak deformations (faulting and local moderate tilting). Our new field observations highlighted significant brittle tectonics, crushed silicified Serouenout sandstones forming locally elongated domes underlining the fault network. The latter (Fig. 5) is dominated by vertical strike-slip faults, mainly N-S (Fig. 1). Some of these strike-slip faults were feeders for the Cenozoic lava flows and were sealed by the basalt, forming dykes.

- The displacements related to the N-S faults are all with dextral component (Fig. 1, 5). This motion is well marked by well-preserved slickenside striations on fault plane (Fig.6) and locally fault hooks. These striations present a weak plunge (12 to 14° northward in average). That indicates fault horizontal displacement associated with a moderate uplift of the eastern compartment relatively to the western one (oblique striations). The figure 4c illustrates the example of such a dextral N010° vertical fault, which is also associated with a vertical movement. West of the fault, Cenozoic flows are lying over the Precambrian granitic basement, implying the local erosion of the whole Serouenout Formation before the volcanism for only the western fault compartment. The vertical

displacement along this fault then corresponds at least to the thickness of this eroded formation, likely of the order of 300 to 350 m. Given this vertical displacement and the 15° dip of the observed slickenside striations within the fault plane, the horizontal displacement must have been of at least 1 km.

- Other large faults with different orientation present two different cases. A N070° strike-slip fault (close to the sites ***f*** – Fig. 1a) is associated with a local tilting (up to 40°) of the Serouenout levels on its southern border. Its fault plane, dipping 75°SE, shows oblique 42° southwestward slickenside striations attesting to a sinistral motion with small reverse component (Fig. 6b). N110° to N120° vertical faults affect the northeastern part of the basin. One of them (along the Oued Tafassasset - Fig. 1), filled by crushed sandstone, shows sub-horizontal slickenside striations indicating a dextral motion. On the southwestern border of the basin (Djebel Taharaq area, located SW of the Adrar Tissèyène – Fig. 1), N120° normal faults, with slide down of northern block, affected the Serouenout Formation before and after the volcanic episode, giving local tilting (Remy, 1959; Aït Hamou, 2000). For Bordet, 1955, such faults could have played a role since the beginning of the basin development.

It is important to underline that N-S vertical faults also affect the Cenozoic lava flows NE of the basin (Fig. 1), giving local moderate tilting. Few dextral sub-horizontal slickenside striations (10° northward in average), not well-preserved, have been also observed on these fault planes.

The moderate dips measured in the Serouenout levels, mainly to the north or south in the basin (Fig. 1), indicate roughly E-W oriented axes for these weak undulations. Local stronger variations in dip are related to tilting associated with faulting. Part of the variations in altitude of the basal levels (Fig. 4a) is also related to faulting (Fig. 4b, c and d). The fault network (Fig. 5) suggests a roughly NNE-SSW maximum stresses direction during the brittle tectonic, but the small number of faults does not allow a rigorous inversion of the dataset

Age and new paleobotanical data

Based on the stratigraphic position of the Serouenout formation, a Cambro-Ordovician age was first suggested (Kilian, 1939; Lelubre, 1952). Bordet (1954) found abundant silicified wood, some of it well preserved. Fragments were identified by Boureau (1952) as *Protopodocarpoxylon Rochii*, similar to woods found in Mid-Cretaceous levels of the Tchad territory. These remnants suggested a Lower Cretaceous to Cenomanian age (Bordet, 1954, 1955; Fabre, 1983; Lefranc and Guiraud, 1990; Philippe et al. 2003). A Lower Cenozoic age for the upper part of the Serouenout Formation was also suggested (oral com. in Fabre, 1983).

The stratigraphic section at the vicinity of the Oued Ounane (24°44' 09", 7°25'29") provided us new evidence to constrain the age of the Serouenout Formation. In the uppermost levels, we discovered, associated with wood fragments, a fern-rich horizon with *Weichselia reticulata* (Fig. 7). *Weichselia reticulata* is a widespread

Mesozoic fern, ranging in age from Bathonian to Cenomanian and geographically between 60°N and 60°S (Barale, 1979; Blanco-Moreno et al. 2018).

Paleomagnetic data

Sampling and analysis procedure

Serouenout Formation coarse facies are mostly not favorable for paleomagnetic studies. However, 24 sites (Fig. 1), distributed in the various levels (Fig. 2) have been sampled in the less coarse facies (247 cores oriented with magnetic and sun compasses). 88 cores, similarly oriented, of Cenozoic volcanic rocks were also collected. To attempt a contact test, a thin (about 30 cm thick) unaltered Cenozoic volcanic dyke, emplaced within a former dextral fault, was sampled (site 18a) and samples from sedimentary host-rocks in contact with it were also collected along two sections perpendicular to the dyke and corresponding to various sedimentary levels (sites 18b1 and 18b2 separated by about 10 m). The site 13 was chosen in a lava flow overlying the sedimentary strata (sampled in the neighboring site 12). 7 of the sedimentary sites (hereafter named sites ***f*** – Fig. 1a) were chosen close to an important dextral fault because of their significant dip. They are however also characterized by clear effects of local intense fluids circulation related to the tectonics (important re-crystallization around the fault).

One to three specimens were cut from each core in order to have additional specimens for pilot studies and rock magnetic analyses. The paleomagnetic study was made in the Algiers CRAAG laboratory. Prior to any demagnetization analysis, the specimens were stored in a zero field for at least one month, to reduce possible viscous components. The remanent magnetization of the specimens was measured using a JR5 spinner magnetometer (AGICO, Brno). Thermal demagnetization was performed using a cylindrical furnace (ASC Model TD48-SC) with a fast-heating rate (45 minutes to reach 680°C) while forced air enhanced the cooling (20 minutes). The directions of the magnetization components were plotted on orthogonal vector plots (As and Zijderveld, 1958; Zijderveld, 1967) and the remaining vectors of the magnetization on equal-area projections. The direction of the different components was computed using principal component analysis (Kirschvink, 1980). Fisher (1953) statistics was used to determine the mean directions.

Thermomagnetic KT curves (low-field magnetic susceptibility K as a function of temperature T) have been measured under air atmosphere for representative samples, with the KLY-3 (AGICO) of the IPGP laboratory. Hysteresis loops were obtained in the IPGP laboratory with the VSM/AGM 3000 (Princeton).

Rock magnetism

The obtained KT curves for sedimentary sites (Fig. 8) are noisy due to the weak susceptibility values. Most of them present a reversible evolution. Perfectly reversible partial cooling loops (Fig. 8) during the heating show that mineralogical alteration occurred only at the highest temperatures (giving a shift of the cooling curve). On the heating curve, a maximum around 300°C is related to a low temperature magnetic phase. It is followed by a regular decrease up to 580°C indicating the presence of the magnetite. A last sharp decrease up to 670°C (preceded in some samples by a small Hopkinson peak), is a characteristic of the presence of hematite. The reversibility of the KT curves indicates that the three evidenced magnetic phases are almost stable during heating, even at high temperature, suggesting Ti-rich titanomagnetite as the lowest temperature one (titanomaghemite or sulphides are generally unstable at high temperature). Owing to the much lower magnetic susceptibility of the hematite compared to that of the Ti-rich titanomagnetite and of magnetite, the latter are present only in moderate proportion.

The measured hysteresis loops for sedimentary samples (Fig. 9) are often noisy. They present typical characteristics (open loops, high remanent coercive force) of high coercivity minerals like hematite. Only some minor wasp-waisted or pot-bellied shapes suggest the presence of the other magnetic components.

Paleomagnetic results

Sedimentary sites

The Natural Remanent Magnetization (NRM) intensity is mostly weak (in 10^{-3} A/m, between 0.4 and 53.7; mean value 8.2). Several pilot specimens were subjected to a stepwise alternating field (AF) demagnetization up to 100 mT or thermal demagnetization up to 680°C to characterize the components of magnetization. AF appeared as totally inefficient and was not further used. Seven of the 24 sampled sedimentary sites (including the site 12 close to the volcanic flow site 13) did not yield reliable results (too weak magnetization to obtain reliable data by principal component analysis). This was also the case for a proportion of the samples from the other sites, and only 80 samples gave usable results, meaning that some sites had a very low number of reliable data. None of these results were later discarded because of inconsistent direction relative to other samples from the same site. In these samples, during thermal demagnetization (Fig. 10) and after elimination of a poorly defined A component mainly related to the present magnetic field (Fig. 11), the analysis of the magnetization mostly evidences the presence of 3 different components B, C and D with very neighboring directions (Tab. 1). All are of normal polarity, except for the C component of reversed polarity in a few samples from a single site (Figs. 10 and 11 – sample SR224A). The difference between the different components, often small, mainly appears on the Zijderveld

plots (Fig. 11). The 4 corresponding demagnetization temperature windows are roughly lower than 250°C (A component), 250-350°C (B), 350-580°C (C) and higher than 580°C (D). The D component is a Characteristic Remanent Magnetization (ChRM).

Except for the site 1, clustering (shown by the precision parameter k - Fisher, 1953) in each site is better for the D component (Tab. 1) for which k is relatively high (mean value: 166). However, the corresponding radius of the confidence zone α_{95} (Fisher, 1953) is relatively large for some sites because of the weak number of obtained data (e.g., 3 for sites 1 and 10). According to the results, different groups of directions can be distinguished (Tables 1 and 2). The sites ***f***, close to a fault and clearly affected by recrystallization, present negative fold test (Figs. 12a, 12b and 13) for all components, with increasing directions scattering, highlighted by the *k* parameter values, from D to C to B components (Tab 2). The site 23, close to another fault, presents directions with large scattering (*k*=10 for component D), probably also disturbed during the faulting. The other sites (hereafter named sites ***s***), widespread in the basin, present on the contrary positive fold test (Figs. 12c, 12d and 13) for all components, but here also with increasing scattering from D to C to B directions (Tab. 2). The fold tests are obviously not significant for the B components, owing to the weak variation of the *k* parameter during progressive untilting, but it can be noticed that this variation has the same evolution (increase or decrease with untilting) as for the corresponding C and D components. This variation is much larger for the C components, and even larger for the D ChRMs, despite weak dip variations from one site to another (Table 1): For the site ***s***, the mean dip value is 10° and dip is mostly towards neighboring directions. Mean dip is 22° for the sites ***f***. For the D ChRMs, the maximum *k* value during progressive untilting is not significantly different from the *k* values for 0% untilting for the sites ***f*** (indicating negative fold test) and 100% untilting for the sites ***s*** (positive fold test). The corresponding ratios *k* maximum/ *k* minimum are 3.7 (sites ***f***) and 2.2 (sites ***s***). The fold tests for the D ChRMs are then fully reliable: D ChRM acquisition is pre-tilting for sites ***s*** and post-tilting for sites ***f***.

The contact test for the site 18 shows that only the boundary of the Serouenout sediments in the contact with the dyke has a perturbed magnetization during dyke emplacement, indicating that the magnetization of these sediments further away from the dyke was acquired before volcanism. Surprisingly, these perturbations are different in the two host rocks sites studied.

- For the samples from the sedimentary site 18b1, a thermal overprint, limited to the first 20 centimeters of the dyke boundary, results only in unreliable scattered directions for the B component. The C and D components remained unaffected. In this narrow boundary, the temperature reached during the dyke intrusion was then lower than most blocking temperatures for these components.

- Within a larger distance to the dyke (about 1 m), all the samples of the sedimentary site 18b2 underwent chemical effects affecting the magnetization. Only B and C components, totally remagnetized, have been obtained (no D component). This likely reflects local effects of active fluids associated with magma emplacement.

This difference in the impacts of the intrusion according to the sites could possibly be related to a greater porosity of the sampled level in the site 18b2 than in the site 18b1?

Volcanic rocks (sites 13 and 18a)

The NRM intensity is much stronger than in sandstones (in A/m, between 1 and 18; mean value 7).

In the partially weathered lava flow (site 13), the thermal demagnetization data suggest that the main magnetic carrier is a Ti-rich titanomagnetite, but also that a part, mostly very small, of the remanence is carried by Ti-poor titanomagnetite. Unfortunately, remanent magnetization is very unstable during thermal treatment, probably because of the weathering effect. Table 1 gives the paleomagnetic direction obtained by AF demagnetization for moderate fields. The relation of this direction with that of the reliable components obtained in the sedimentary sites is unclear.

In the dyke (site 18a), the thermal demagnetization (Fig. 10) clearly indicates both Ti-rich and Ti-poor titanomagnetites. However, the corresponding paleomagnetic directions are unreliable due to their strong scattering, suggesting lightning disturbances.

Discussion

Magnetic mineralogy

The presence of primary or secondary magnetite (here in small amounts) in red beds is not surprising (e.g., Miller and Folk, 1955; Turner, 2009; Bilardello and Kodama, 2010). The occurrence of Ti-rich titanomagnetite, even like here in very weak amounts, is more unusual. The presence of this mineral in the Cenozoic volcanic rocks suggests a possible relationship with the migration of chemically rich volcanic fluids throughout the whole sedimentary basin.

The components B, C and D and the sites f and s

The temperature windows, associated with the different B, C and D components and those of the variations highlighting Ti-rich titanomagnetite, magnetite and hematite on the KT curves, are similar, showing that the different components B, C and D are connected with the magnetic mineralogy. However, for sites ***s*** and ***f,*** the proximity of the direction for the different components clearly indicates a close relationship between them. In addition, in a few samples, the C component is very weak, or even in the opposite direction to the D ChRM, then clearly due to the superposition of magnetizations of opposite polarity carried by hematite and magnetite (Fig. 11

samples SR28A and SR96A). B and C components are therefore composite magnetizations, resulting from the superposition of the hematite magnetization with that of magnetite (C component), and with those of magnetite and Ti-rich titanomagnetite (B component). Such superpositions also explain the larger scattering directions in the B and C composite components relatively to the D ChRM (Tab. 2). Obtention of linear segments for B and C components on the Zijderveld plots then shows that the different component minerals phases are demagnetized in relatively regular proportions during the corresponding temperatures intervals (e.g., Derder et al. 2022). Hematite clearly remains the dominant carrier in most cases, with Ti-rich titanomagnetite and magnetite being carriers of partial remagnetizations. Composites B and C components will be therefore not further considered. This highlights the importance of a detailed analysis of the demagnetization data for rocks with different magnetic phases.

As shown by the negative fold test, the D ChRM is a remagnetization (e.g., Henry et al. 2004) in sites ***f*** affected by intense fluids circulation close to the fault (see Yang et al. 2019), while the positive fold test for the sites ***s*** argues for a primary magnetization.

Paleomagnetic dating

The seven sites ***s*** are well distributed in the basin and stratigraphically located in the 2/3 lower levels of the formation (Figs. 1 and 2). Their D ChRM (Ds= 343.8°, Is= 15.5°, k= 140, α_{95}= 5.1° after tilt correction, Fig. 12) was used to determine a paleomagnetic pole (67.2°S, 53.6°E with K = 166, A_{95}= 4.1°) for the Serouenout Formation. Such a pole would not have been used to improve an APWP, owing to the low number of obtained results (only 31 data for 247 samples, from 7 sites out of 24), far from the paleomagnetic standards. However, considering its uncertainty, it can be compared (Fig. 14) with the APWP for Africa (Besse and Courtillot, 2002; Domeier et al. 2012, modified from Le Goff et al. 1992; Amenna et al. 2014; Henry et al. 2017) to estimate the acquisition age of its ChRM. In order to obtain a clear and reliable comparison, the variation of the absolute angular difference between this Serouenout pole and the APWP as a function of age (every 10 Ma) was determined (blue curve on the figure 15a). Angular uncertainties A_{95} from our pole and from each mean pole of the APWP was integrated (green and red curves delimiting the corresponding uncertainty zone on the figure 15a). For the age of magnetization acquisition, this indicates two possible age windows, corresponding to the Triassic (before 198 Ma) and Upper Cretaceous-Lower Paleocene (95-62 Ma) ages. For the Serouenout Formation, a Triassic age is not compatible with the known paleobotanical data (Upper Jurassic to Cenomanian). On the contrary, the coincidence (Fig. 15a) of the age windows for these latter data and for the ChRM acquisition (Upper Cretaceous-Lower Paleocene) suggests a primary magnetization for these sediments, which strongly favors a Cenomanian deposition of the formation. It should be noted that Kilian (1930) found the ammonite *Calycoceras naviculare*, of Cenomanian

age (Busson et al. 1999), in the Amguid limestones (also discordant on the Precambrian basement, but in a completely different context - marine transgression - e.g., Kocsis and Scotese 2020) in the North Hoggar. For Lelubre (1952), these Amguid levels were deposited in an area with large valleys, suggesting an earlier tectonic episode within the leveled Hoggar shield.

The post-tilting D ChRM of the 7 sites ***f*** (Dg= 349.4°, Ig= 26.7°, k= 82, α_{95}= 6.7° before tilt correction) was used to determine a paleomagnetic pole (Latitude = 75.7°S, Longitude = 52.3°E, K = 112, A_{95}= 5.0°) for the remagnetization age (Fig. 14). The same approach using the absolute angular difference with the APWP (Fig. 12b) gives, for remagnetization acquisition, a Coniacian - Eocene age window (101-35 Ma – Fig. 14). The other possible window - lower Mesozoic age 176-190 Ma – for remagnetization acquisition is here also not compatible with the geological data. Tectonics, with tilting and faulting, then occurred during the Upper Cretaceous - Eocene, at least in the sampled area including the sites ***s***.

Structural implications

The presence of the relatively thick detrital Serouenout Formation (up to 350 m), deposited within a large area, suggests the existence of a prior significant topography. In addition, Bordet (1955) observed that the Serouenout bottom levels locally filled ridged depressions. He also noticed, as indicated above, that N120° normal faults could have played a role since the beginning of the basin development. The basal conglomerate with very large pebbles (Fig. 3) indicates that the eroded reliefs were not very far from the basin. These different field observations reveal a tectonic event shortly before the deposition of the Serouenout sandstones.

The observed tectonic brittle deformation postdates the deposition of the Serouenout Formation. This event generated local moderate tilting and, along vertical faults, significant displacements lateral and vertical in a N-S dextral shearing context. The paleomagnetic directions obtained in the different sites are well-clustered (confidence zones partly included within the confidence zone for the mean direction), except for the site 3 (Fig. 12e); this could indicate a moderate local clockwise rotation undergone by this last site, in agreement with such a context. The moderate reverse displacement along a fault suggests a compressive context. The shearing along the different strike-slip faults and the approximately E-W undulation axes in the basin suggest that these deformations are related to a sub-horizontal maximal stress direction roughly oriented SSW-ENE. Volcanism sealing tectonic structures (Fig. 4c) suggests faulting prior to this Oligocene volcanism (34-17 Ma). This is also evidenced by the presence of basaltic dykes sealing strike-slip faults within the Serouenout Formation and by the post-tilting possible remagnetization age (89-35 Ma) of the sites ***f***.

The lava flows covering the Serouenout Formation were also affected latter by N-S dextral strike-slip faults and locally by weak tilting. In the Tirhitine area (200 km to the east of Serouenout), Kettouche et al. (2013) and Maouche et al. (2014), using field investigation highlighted that sedimentary Oligocene - Early Miocene formations (Rognon et al.1983) are affected by numerous kilometric faults (with N-S, NE-SW and NW-SE dominant directions) similarly as the Serouenout Formation. These observations could reflect a structural setting similar to the one here described in the Serouenout area, suggesting a regional and temporal extension of the shearing context during the Neogene. This Neogene structural setting could be related to the convergence between Africa-Europe since the Oligocene, resulting in Alpine reactivations of N-S Pan-African mega-shear zones, as well as Cenozoic Atakor volcanic activity (Liégeois et al. 2005; Azzouni-Sekkal et al. 2007) on the boundaries of LATEA metacraton (Liégeois et al. 2003). Similar reactivation during the Variscan orogeny (e.g., Haddoum et al. 2001, 2013; Haddoum, 2009) and current intraplate earthquake activity confirm that these mega-shear zones constitute mechanically weak area that may deform in response to distant tectonic events (Boughacha, 2005; Harbi 2006). Similarly, the Cenomanian tectonic activity could be linked to the Pangea dislocation and South Atlantic opening, a period that favored the Cretaceous West and Central African Rift System (e.g., Ghomsi et al 2022).

Conclusion

Age characterization of the Serouenout Formation suggest that it has been deposited in a large area during Cenomanian probably in response to tectonic faulting. The tectonic record in this formation shows a succession of faulting events during the Cenomanian and the Cenozoic. These events correspond for the Precambrian basement of the Hoggar to a new and "recent" page of its structural history, which is difficult to evidence in such old cratons where Meso-Cenozoic sedimentary record is often lacking. The Cenozoic uplift of the Hoggar (Rougier et al. 2013) thus cannot be considered as a simple global vertical movement. (Liégeois et al.2005). During Cenomanian, local differential uplifts occurred probably controlled by a tectonic extensional event. During Cenozoic, the Hoggar uplift was accompanied by tectonic tilting and faulting with horizontal dextral component, then, constituting an example of interaction of uplifts at various scales and of a continuum of Alpine reactivations of Pan-African mega-structures.

Acknowledgements

This work was supported by the Algerian–French cooperation CMEP- PHC "Tassili" program 12MDU878. Many thanks to the Algerian DPGRF of the MESRS and to the French Foreign Office for their help. We are very grateful to Jean-Paul Liégeois for his detailed and constructive review

Declarations

Conflict of interest : The authors declare that they have no competing interests

References

Ahmed Y, Konaté M, Harouna M (2016) Tectono-magmatic reactivation of Téfidet Cretaceous trough during Cenozoic (Aïr, Niger). Bull Soc géol France, 187: 73-82

Aït Hamou F (2000) Un exemple de "point chaud" intracontinental en contexte de plaque quasi-stationnaire : étude pétrologique et géochimique du Djebel Taharaq et évolution du volcanisme cénozoïque de l'Ahaggar (Sahara algérien). Thesis, University, Montpellier

Aït-Hamou F, Dautria JM (1994) Le magmatisme cénozoïque de l'Ahaggar : une synthèse des données disponibles. Mise au point sur l'hypothèse d'un point chaud. Bull Serv Géol Algérie 5: 49–68

Aït-Hamou F, Dautria JM, Cantagrel JM, Dostal J, Briqueu L (2000) Nouvelles données géochronologiques et isotopiques sur le volcanisme cénozoïque de l'Ahaggar (Sahara algérien) : des arguments en faveur de l'existence d'un panache. Compt Rend Acad Sci Paris, Sci Terre planètes, 330: 829–836

Amenna M, Derder MEM, Henry B, Maouche S, Bayou B, Bouabdallah H, Ayache M, Bediaf M (2014) Improved Moscovian part of the Gondwana APWP for paleocontinental reconstructions, obtained from a first paleomagnetic pole, age-constrained by a fold test, from In Ezzane area in the Murzuq basin (Algeria, stable Africa). J Afr Earth Sci 99: 342–352

As JA, Zijderveld JDA (1958) Magnetic cleaning of rocks in paleomagnetic research. Geophys J Roy Astron Soc 1: 308-319

Azzouni-Sekkal A, Bonin B, Benhalou A, Yahiaoui R, Liégeois JP (2007) Tertiary alkaline volcanism of the Atakor, Hoggar, Algeria.Geol Soc America, Spec Pap 418: 321-340

Barale G (1979) Découverte de Weichseliareticulata (Stokes & Webb) Fontaine emend. Alvin, filicinée leptosporangiée, dans le Crétacé Inférieur de la province de Lérida (Espagne): implications stratigraphiques et paléoécologiques. Geobios 12: 313–319

Baziz K, Liégeois JP, Azzouni-Sekkal A (2005) La carte géologique Asséo au 1/200 000: structure, Pétrologie et Géochronologie de deux “Terranes” Issalane et Sérouènout dans le S. E. Hoggar (Algérie). Séminaire de géologie et de métallogenie des massifs du Hoggar et des Eglab, Tamanrasset, Algérie

Beccaluva L, Azzouni-Sekkal A, Benhallou AZ, Bianchini G, Ellam RM, Marzola M, Siena F, Stuart FM (2007) Intracratonic asthenosphere upwelling and lithosphere rejuvenation beneath the Hoggar swell (Algeria): Evidence from HIMU metasomatised lherzolite mantlexenoliths. Earth Planet Sci Lett 260: 482-494

Benhallou AZ, Megueni Y, Boussisse F, Ikhlef-Debabha F, Babkar Y, Boukhalfa Z, Aghanbilou K, Azzouni-Sekkal A, Dautria JM (2019) The South-West Atakor volcanic district (Hoggar): Petrography and mineralogy from the Taessa lavas. Proc 1st Springer Conf Arab J Geosci (CAJG-1) Tunisia 2018, Adv Sci Techn Innov, Springer Intern Pub 29–32. https://doi:10.1007/978-3-030-01575-6_7

Besse J, Courtillot V (2002) Apparent and true polar wander and the geometry of the geomagnetic field over the last 200 My. J Geophys Res 107, 2300. https://doi:10.1029/2000JB000050

Bilardello D, Kodama KP (2010) Palaeomagnetism and magnetic anisotropy of Carboniferous red beds from the Maritime Provinces of Canada: evidence for shallow palaeomagnetic inclinations and implications for North American apparent polar wander. Geophys J Intern 180: 1013-1029

Black R, Latouche L, Liégeois JP, Caby R, Bertrand JM (1994) Pan-African displaced terranes in the Tuareg Shield (central Sahara). Geology 22: 5-16

Blanco-Moreno C, Gomez B, Buscalioni AD (2018) Paleobiogeographic and metric analysis of the Mesozoic fern Weichselia. Geobios 51: 571-578

Blanco-Moreno C, Decombeix AL, Prestianni C (2020) New insights into the affinities, autoecology, and habit of the Mesozoic fern Weichselia reticulata based on the revision of stems from Bernissart (Mons Basin, Belgium). Pap Palaeontology spp2 1344. doi:10.1002/spp2.1344C

Bordet P (1954) La série de Sérouenout (Ahaggar oriental) est d’âge "Continental intercalaire" (Crétacé moyen). Compt Rend hebdo Scéanc Acad Sci Paris 238: 500-503

Bordet P (1955) La série de Sérouenout (Continental intercalaire) et son substratum précambrien en Ahaggar oriental. Bull Serv Carte Géol Alg, Nouvelle série 5: 7-10

Boudjema A, Tremolières P (1988) The role of the structural heritage and global tectonic events in the evolution of the Algerian Triassic Basin: tectonic inversion and reservoir distribution. AAPG Annual Conv, Houston, Texas

Boughacha MS (2005) Analyse de la sismicité de l'Algérie. Application à l'établissement des cartes des I.M.O et ΔCFF. Thesis, University, Alger 289 pp

Boureau E (1952) Étude des fossiles du Territoire du Tchad: 1. Protopodocarpoxylon rochii n. sp. Bois fossile mésozoïque. Bull Mus Hist Nat Paris 24: 223-232

Busson G, Dhondt A, Amédro F, Néraudeau D, Cornée A (1999) La grande transgression du Cénomanien supérieur-Turonien inférieur sur la Hamada de Tinrhert (Sahara algérien): datations biostratigraphiques, environnement de dépôt et comparaison d'un témoin épicratonique avec les séries contemporaines à matière organique. Cretac Res 20: 29–46

Craig J, Rizzi C, Said F, Thusu B, Lüning S, Asbali AI, Keeley ML, Bell JF, Durham MJ, Eales MH, Beswetherick S, Hamblett C (2008) Structural styles and prospectivity in the Precambrian and Palaeozoic hydrocarbon systems of North Africa. In: Salem MJ (Ed.) The Geology of East Lybia (4). Gutenberg Press, Malta :51-122

Dautria JM, Lesquer A (1989) An example of the relationship between rift and dome: recent geodynamic evolution of the Hoggar swell and of its nearby regions (Central Sahara, Southern Algeria and Eastern Niger). Tectonophysics 163: 45-61

Derder MEM, Henry B, Maouche S, Ammena M, Bayou B, Djellit H, Guemache MA, Hemmi A (2009) New structural implications for central Sahara (Algeria) from revisited Upper Carboniferous "HassiBachir" formation: Paleomagnetic constraints. Tectonophysics 463: 69-76. doi:10.1016/j.tecto.2008.09.012

Derder MEM, Henry B, Maouche S, Amenna M, Ouabadi A, Bayou B, Bestandji R, Bouabdallah H, Ayache M, Beddiaf M (2022) Enigmatic well-characterized remanent magnetization of silicified Lower Devonian rocks from the Tadrart area (Murzuq basin, SE Algeria). Intern J Earth Sci 111: 1185-1200. doi.10.1007/s00531-022-02173-6

Derder MEM, Maouche S, Missenard Y, Henry B, Ammena M, Ouabadi A, Bayou B, Bestandji R, Kettouche J, Haddoum H (2023) Combined paleomagnetic and paleobotanical dating of the "Serouenout" sedimentary cover in the NE of the Hoggar shield (Algeria): Structural implications. ICES 2023. Riyadh, Saudi Arabia.

Domeier M, Van der Voo R, Torsvik TH (2012) Paleomagnetism and Pangea: The road to reconciliation. Tectonophysics 514-517: 14-43

Fabre J (1983) Afrique de l'Ouest. Introduction géologique et termes stratigraphiques. Pergamon 396 pp

Faure H (1985) Aspects généraux du Tertiaire et du Quaternaire de l'Afrique.CIFEG Paris.

Fisher RA (1953) Dispersion on a sphere. Proc Roy Soc London A 217: 295-305

Ghomsi FEK, Tenzer R, Njinju E, Steffen E (2022) The crustal configuration of the West and Central African Rift System from gravity and seismic data analysis. Geophys J Intern 230: 995–1012, doi.org/10.1093/gji/ggac089

Guiraud R, Bosworth W, Thierry J, Delplanque A (2005) Phanerozoic geological evolution of Northern and Central African: an overview. J Afric Earth Sci 43: 83-143

Haddoum H, Guiraud R, Moussine-Pouchkine A (2001) Hercynian compressional deformations of the Ahnet-Mouydir Basin, Algerian Saharan Platform: far-field stress effects of the late Palaeozoic orogeny. Terra Nova 13(3): 214-219

Haddoum H (2009) Les structures hercyniennes dans la couverture sédimentaire paléozoïque de l'Ahnet occidental et de Bled El Mass (N.O. Hoggar, Algérie): une conséquence du rejeu des failles panafricaines. Bull Serv Géol National 20(3): 221-243

Haddoum H, Mokri M, Ouzegane K, Ait-Djaffer S, Djemai S (2013) Extrusion du bloc In Ouzzal-vers le Nord (Hoggar Occidental Algérie): Conséquence d'un poinçonnement-Panafricain. J Hydrocarb Mines Environ Res 2013, 4: 6-16

Harbi A (2006) Évaluation de l'aléa sismique en Algérie du Nord par la modélisation de l'input sismique dans les zones urbaines et l'établissement d'un catalogue. PhD Thesis, University, Algiers

Henry B, Merabet N, Derder MEM, Bayou B (2004) Chemical remagnetizations in the Illizi basin (Saharan craton, Algeria). Geophys J Intern 156: 200-212

Henry B, Derder MEM, Ammena M, Maouche S, Bayou B (2017) Better constrained selection of the Paleozoic West Gondwana (South America) paleomagnetic poles for the APWP's determination. Stud Geophys Geod 61: 185-198. doi: 10.1007/s11200-016-1036-9

Kettouche D, Maouche S, Haddoum H , Khaldi A, Derder MEM, Nacer J, Ouabadi A, Missenard Y, Rougier S (2013) Evidence of Post Cenozoic Tectonics in the Hoggar Shield (South Algeria). Geophys Res Abstracts 15, EGU2013-9927, EGU Gen Assemb 2013

Kilian C (1930) Du Crétacé du versant Nord du Massif Central Saharien. Compt Rend Som Soc Géol France 12: 125

Kilian C (1939) In "Carte Géologique Internationale de l'Afrique". Bureau d'études géologiques et minières coloniales. Institut cartographique de Paris

Kirschvink JL (1980) The least-squares line and plane and the analysis of palaeomagnetic data. Geophys J Roy Astron Soc 62: 699-718

Kocsis A, Scotese CR (2020) Mapping paleocoastlines and continental flooding during the Phanerozoic. Earth-Science Reviews 213, 103463

Lefranc J, Guiraud R (1990) The continental intercalaire of northwestern Sahara and its equivalents in the neighbouring regions. J Afric Earth Sci 10: 27-77

Le Goff M, Henry B, Daly L (1992) Practical method for drawing VGP paths. Phys Earth Planet Inter 70: 201-204

Lelubre M (1952) Recherches sur la géologie de l'Ahaggar, central et occidental (Sahara Central). Bull Serv Carte Géol Algérie 22

Lesquer A, Bourmatte A, Dautria JM (1988) Deep structure of the Hoggar domal uplift (central Sahara, south Algeria) from gravity, thermal and petrological data. Tectonophysics 152: 71-87

Liégeois JP (2019) A New Synthetic Geological Map of the Tuareg Shield: An Overview of Its Global Structure and Geological Evolution. In: Bendaoud A, Hamimi Z, Hamoudi M, Djemal S, Zoheir B (Eds) Geology of the Arab World. an overview. Springer, Cham, pp 83-107. doi.org/10.1007/978-3-319-96794-3_2

Liégeois JP, Latouche L, Boughrara M, Navez J, Guiraud M (2003) The LATEA metacraton (Central Hoggar, Tuareg shield, Algeria): behaviour of an old passive margin during the Pan-African orogeny. J Afric Earth Sci 37: 161-190

Liégeois JP, Benhallou AZ, Azzouni-Sekkal A, Yahiaoui R, Bonin B (2005) The Hoggar swell and volcanism: Reactivation of the Precambrian Tuareg Shield during Alpine convergence and West African Cenozoic volcanism. In: Foulger GR, Natland JH, Presnall DC, Anderson DL (Eds) Plates. Plumes and Paradigms. Geol Soc America, spec paper 388: 379-400

Louis P, Rechenmann J (1966) Interprétation géologique de certaines anomalies gravimétriques du Ténéré (République du Niger). Compt Rend Acad Sci Paris 263: 476-479

Maouche S, Kettouche D, Haddoum H, Derder MEM, Ouabadi A, Missenard Y, Abdallah N, Amenna M, Khaldi A (2014) Post Cretaceous tectonic evolution of the intraplate "Serouanout Basin" (Hoggar Shield, Algeria). Geophys Res Abstracts 16, EGU2014-11878, EGU Gen Assemb

Maurin JC, Guiraud R (1993) Basement control in the development of the Early Cretaceous West and Central African Rift System. Tectonophysics 228: 81-95

Miller DN, Folk RL (1955) Occurrence of detrital magnetite and ilmenite in red sediment: New approach of significance of redbeds. AAPG Data pages 39: 338-345

Monje Durán C, Martínez C, Escapa I, Madriñán S (2016) Nuevos registros de helechos y coníferas del Cretácico Inferior en la cuenca del Valle Superior del Magdalena, Colombia. Bolet Geolog, Univer Industrial Santander 38: 29-42

Nouar O, Henry B, Liégeois JP, Amenna M, Derder MEM, Abdallah N, Ayache M (2021) Evidence of the Murzuq event in the Central Hoggar: Sinistral displacement along the NNW-SSE West-Ounane major shear zone (Gour Oumellalen, Algeria) shown by the magnetic fabric of the Tisseliline pluton. J Afric Earth Sci 184, 104333, doi:10.1016/j.jafrearsci.2021.104333

Ouzegane K, Liégeois JP, Doukkari S, Kiénast JR, Arab A, Drareni A, Gärtner A, Linnemann U (2023) The Egéré Paleo-Mesoproterozoic rifted passive margin of the LATEA metacraton (Central Hoggar, Tuareg Shield, Algeria) subducted and exhumed during the Pan-African orogeny: U-Pb zircon ages, P-T-t paths, geochemistry and Sr-Nd isotopes. Earth-Sci Rev 236, 104262, doi.org/10.1016/j.earscirev.2022.104262

Philippe M, Cuny G, Bamford M, Jaillard E, Barale G, Gomez B, Ouaja M, Thévenard F, Thiébaut M, VonSengbusch P (2003) Metapodocarpoxylonlibanoticum (Edwards) Dupéron-Laudoueneix et Pons and Late Jurassic – EarlyCretaceous continental biogeography J Biogeogr 30: 389-400

Remy JM (1959) Etude géologique et pétrographique du Sud-Est de l'Amadror en Ahaggar (Sahara central) 1959. Thesis, Paris 189p

Rognon P, Gourinard Y, Bandet Y, Koeniguer JC, Delteil-Desneux F (1983) Précisions chronologiques sur l'évolution volcano-tectonique et géochronologique de l'Atakor (Hoggar): Apports des données radiométriques (K/Ar) et paléoclimatique du Plio-Pleistocène Africain. Bull Géol France XXV 6: 973–980

Rougier S (2012) Interactions lithosphère – asthénosphère et mouvements verticaux : le cas du massif du Hoggar. Thesis, University, Paris Sud - Paris XI

Rougier S, Missenard Y, Gautheron C, Barbarand J, Zeyen H, Liégeois JP, Bonin B, Ouabadi A, Derder MEM, Frizon de Lamotte D (2013) Eocene exhumation of the Tuareg Shield (Sahara, Africa). Geology 10.1130/G33731.1

Smith B, Derder MEM, Henry B, Bayou B, Ammena M, Djellit H, Yelles AK, Garces M, Beamud E, Callot JP, Eschard R, Chambers A, Aifa T, Ait Ouali R, Gandriche H (2006) Relative importance of the Hercynian and post-Jurassic tectonic phases in the Saharan platform: a palaeomagnetic study of Jurassic sills in the Reggane basin (Algeria). Geophys J Inter 167: 380-396

Turner P (2009) The palaeomagnetic evolution of continental red beds. Cambridge Univ Press.

Yang T, Chu YM, Ferré E, Dekkers M, Chen J, Yeh EC, Tanikawa W (2019) Faulting processes unveiled by magnetic properties of fault rocks. Rev Geophys. https://doi.10.1029/2019RG000690

Zhou L, Su J, Dong X, Shi B, Sun Z, Qian M, Lou D,Liu A (2017) Controlling factors of hydrocarbon accumulation in Termit rift superimposed basin, Niger. Petrol Explor Develop 44 : 358–367

Zijderveld JDA (1967) AC demagnetisation of rocks: analysis of results. In: Collinson DW, Creer KM, Runcorn SK (Eds) Method in paleomagnetism. Elsevier. Amsterdam: 254-286.

Figure captions

Figure 1: (**a**) Geological map of the Serouenout region (modified from Bordet, 1955 and Derder et al. 2023) and sampling sites locations. Inset indicates the location of the studied area in Algeria.

(**b**) Tectonic setting: post-Cenomanian faults.

Figure 2: Lithological section of the Serouenout Formation at Tin Adakitine (the conglomerate level, not visible in this zone, has been added). The symbols fossils correspond to the levels with ferns (1) and silicified woods (2) observed in other sections in the basin (Fig. 1). The circled numbers indicate the levels corresponding to those of the paleomagnetic sites widespread in the basin (Fig. 1).

Figure 3: Basal conglomerate, including some pebbles larger than 20 cm, lying over the basement (location indicated on the figure 1a).

Figure 4: Evidence of post-Cenomanian tectonics: cross-sections highlight brittle tectonics (see Fig. 1a for positions). The cross-section (c) and its above associated picture presents an example of a dextral vertical N010 fault, also showing an important vertical shift. Scale in meters.

Figure 5: Slickenside striations (dots with arrow) and fault plane: dextral (blue) and sinistral (red) strike-slip faults, and faults without observable slickenside striations (black). Equal-area plot, lower hemisphere.

Figure 6: Examples of observed and measured faults: (a) N-S right lateral strike slip (b) N070 Left lateral strike slip with reverse component. Fault plane (f) and slickenside striations (p) orientation.

Figure 7: (a) *Weichselia reticulata* (Barale, 1979; Monje Durán et al. 2016; Blanco- Moreno et al, 2018, 2020), and (b) silicified wood from the Serouenout Formations.

Figure 8: Typical thermomagnetic curve (normalized low field susceptibility K/K_o as a function of the T temperature): samples SR27 and SR66. Heating (red line) and cooling (dark blue line) curves

Figure 9: Hysteresis loops (samples SR92and SR318), displaying large open loops and showing no reached magnetization saturation. Hcr is the remanent coercive force, Field in Tesla (T) and magnetization is in A/m.

Figure 10: Typical thermal demagnetization curves (normalized Magnetization M/M_0 as a function of the temperature T): variation of the resultant moment in blue and of the total magnetization (from the sum of the lost magnetizations) in red, for the sedimentary sequences (sample SR224) and volcanic dyke (sample SR235 - superposed blue and red curves).

Figure 11: Orthogonal vector plots (filled circles: horizontal plane, crosses: vertical plane; stratigraphic coordinates) and demagnetization curves for samples SR28A, SR62A, SR96Aand SR224A. C component is reversed for SR224A, and weak for SR28A and SR96A, because of superposition of normal (hematite) and reversed (magnetite) magnetizations.

Figure 12: ChRM equal-area plots (lower hemisphere): Paleomagnetic directions, before (a, c) and after tilt correction (b, d), for the sites ***f*** (a, b) and ***s*** (c, d). Mean site data for the sites ***s*** after tilt correction (e), with associated confidence zones α_{95}. Present day magnetic field (PDMF).

Figure 13: Variation of the *k* parameter (Fisher, 1953) during progressive untilting for the B and C components and the D ChRM, for the sites ***s*** (blue) and ***f*** (red).

Figure 14: Comparison of the Serouenout poles for sites ***s*** (red) and ***f*** (green) with the Gondwana APWP (230-210 Ma - Domeier et al. 2012 modified from Le Goff et al. 1992 - and 200-0 Ma - Besse and Courtillot, 2002). To have a clear figure, only confidence zones for Serouenout poles are presented. Effects of uncertainties associated with APWP poles are considered in the figure 12.

Figure 15: In red, possible age windows for deposition (a) and tectonic deformation (b) of the Serouenout Formation. Absolute angular deviation (modified from Derder et al. 2023), as a function of the age (every 10 Ma), between the Serouenout pole and the African APWP (blue curve, the green curves defining the uncertainty angle). Age window for *Weichselia reticulata* in orange.

Table 1: Mean A, B, C and D components in the different sites: Dip P, dip direction G, Number of samples N, Declination and Inclination before (Dg, Ig) and after (Ds, Is) tilt correction and Fisher (1953) parameters k and α_{95}. Sites ***s*** (white background), ***f*** (pinky beige), 23 (green) and volcanism related (blue).

Table 2: Sites mean directions (see table 1) and corresponding paleomagnetic poles (Latitude λ and longitude φ) for the different components.

Figure 2

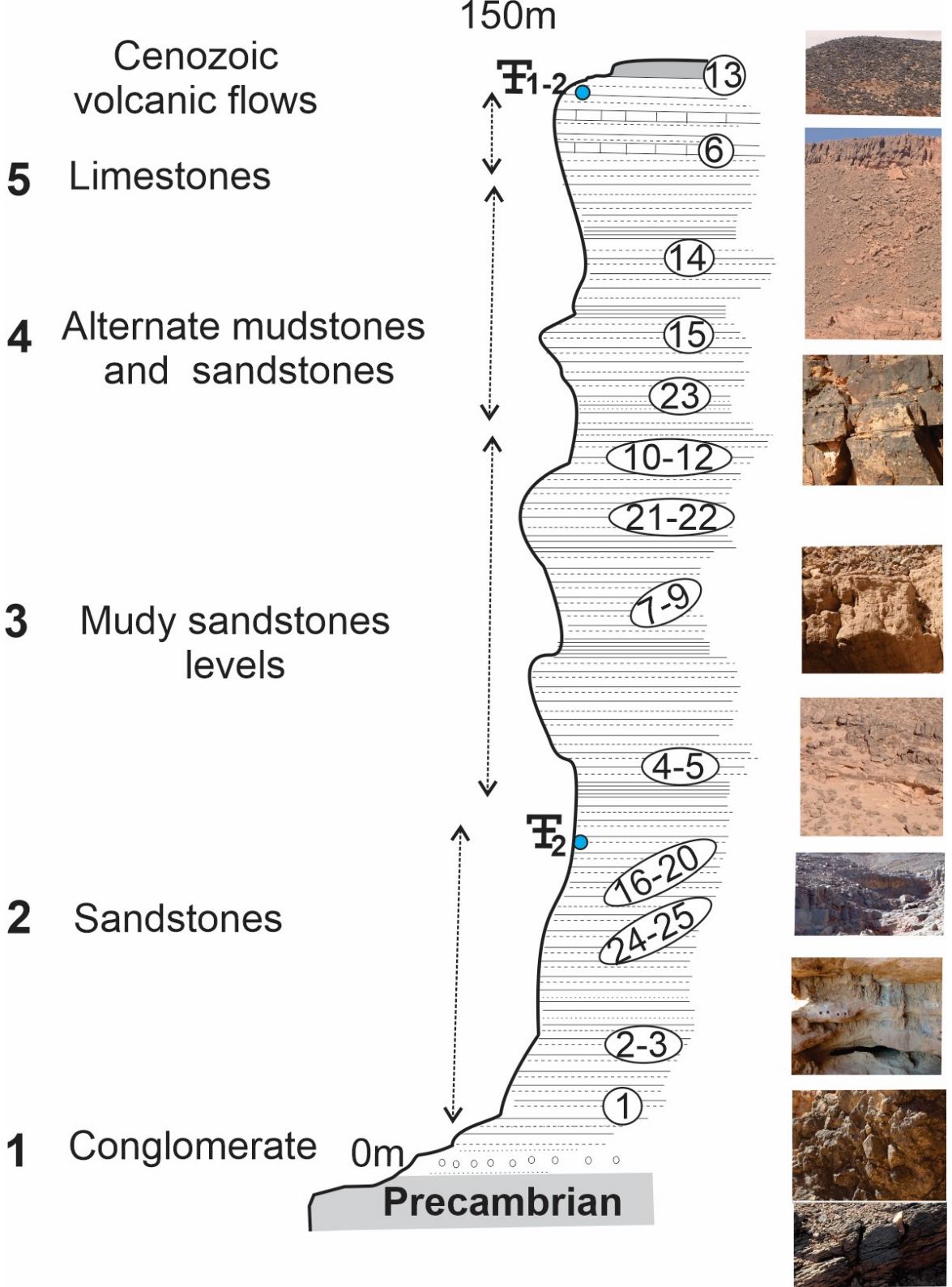
150m
Cenozoic volcanic flows
5 Limestones
4 Alternate mudstones and sandstones
3 Mudy sandstones levels
2 Sandstones
1 Conglomerate
0m
Precambrian
F1-2
F2
13
6
14
15
23
10-12
21-22
7-9
4-5
16-20
24-25
2-3
1

Figure 3

Figure 4

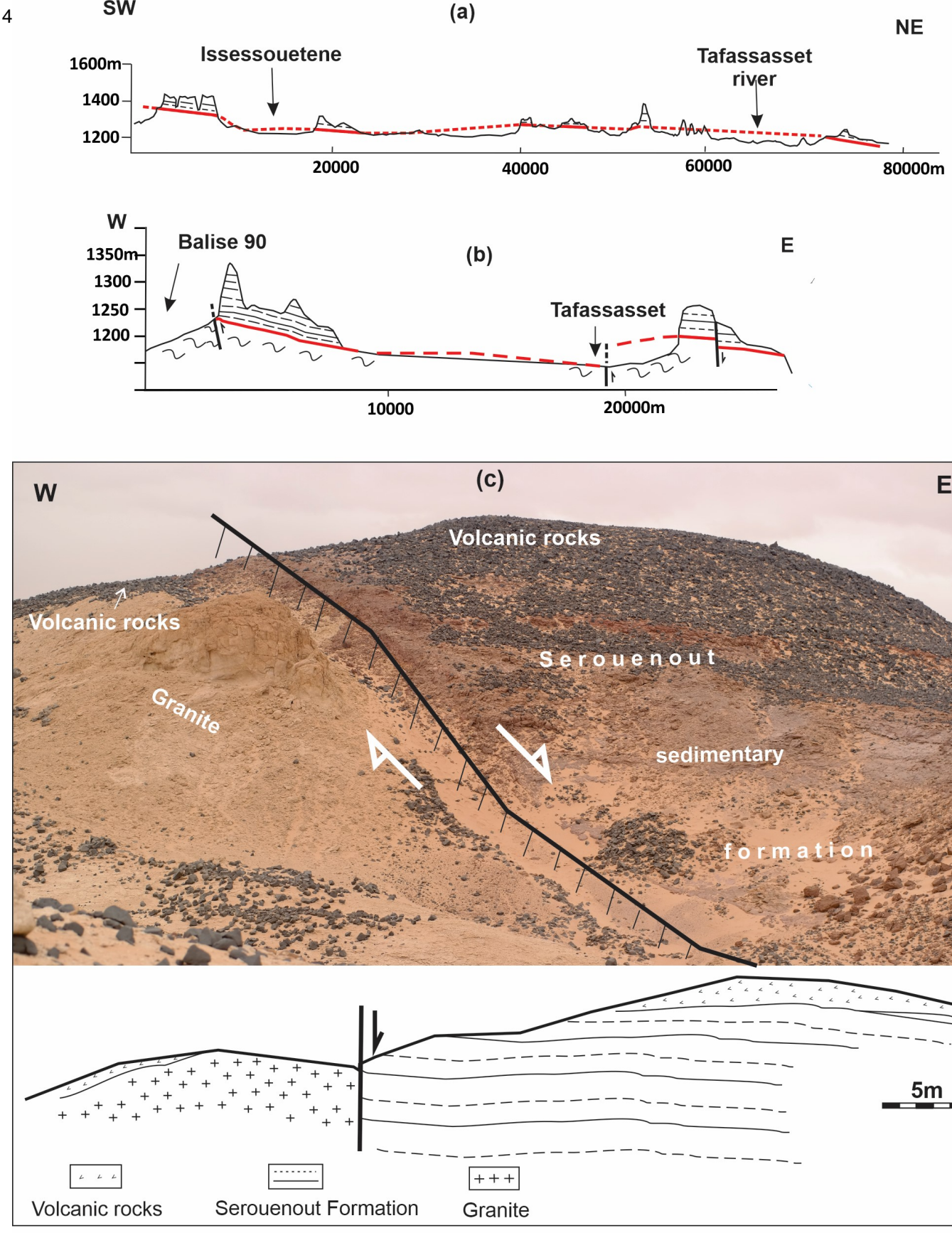
SW
(a)
NE
Issessouetene
Tafassasset river
1600m
1400
1200
20000
40000
60000
80000m
W
Balise 90
(b)
E
1350m
1300
1250
1200
Tafassasset
10000
20000m
W
(c)
E
Volcanic rocks
Volcanic rocks
Granite
Serouenout
sedimentary
formation
5m
Volcanic rocks
Serouenout Formation
Granite
N
(d)
S
1300m
1260
1220
1180
1140
1000
2000
3000
4000m
Serouenout Formation
Basement (Precambrian)

Figure 5

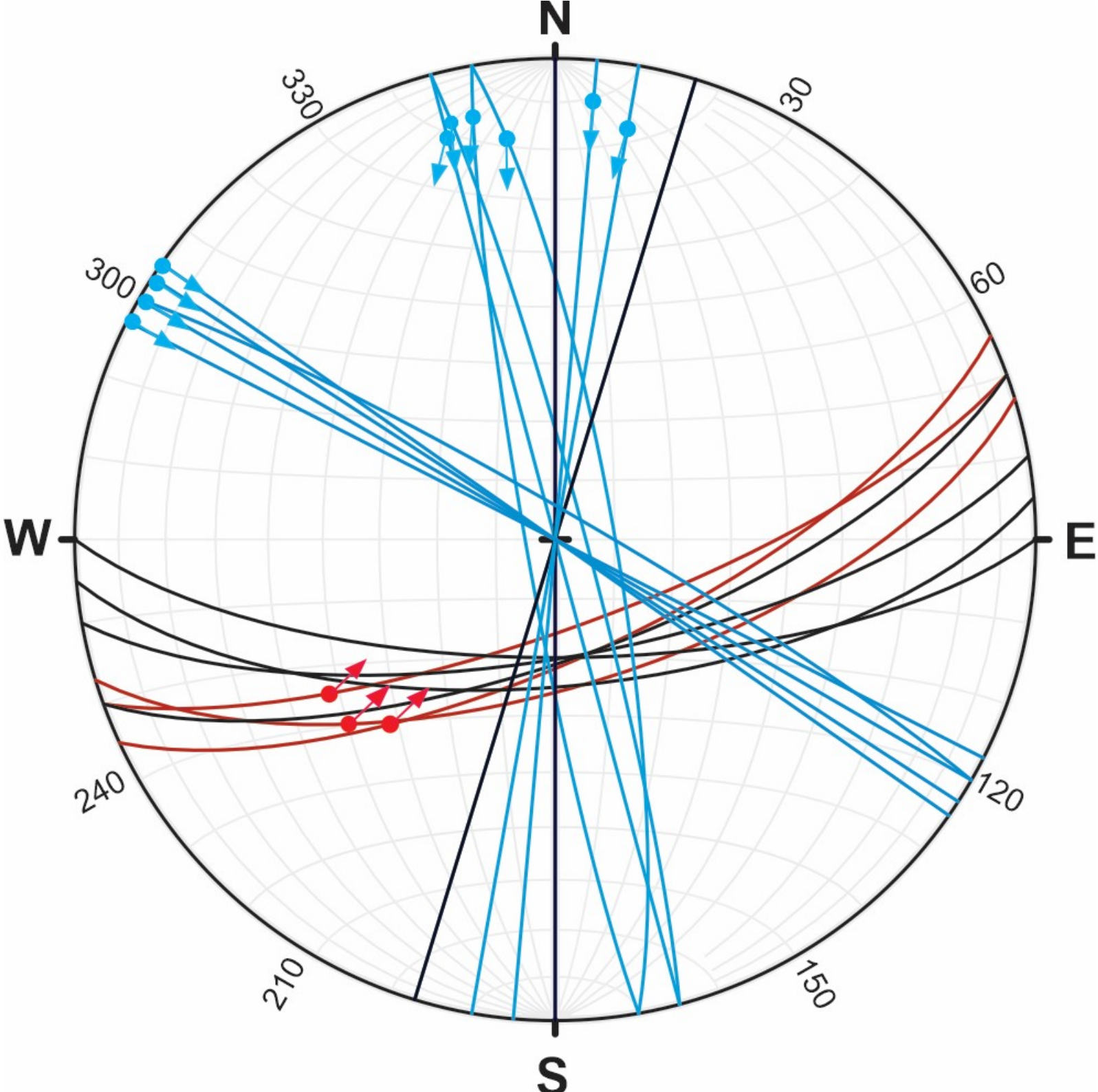

Figure 6

Figure 7

Figure 8

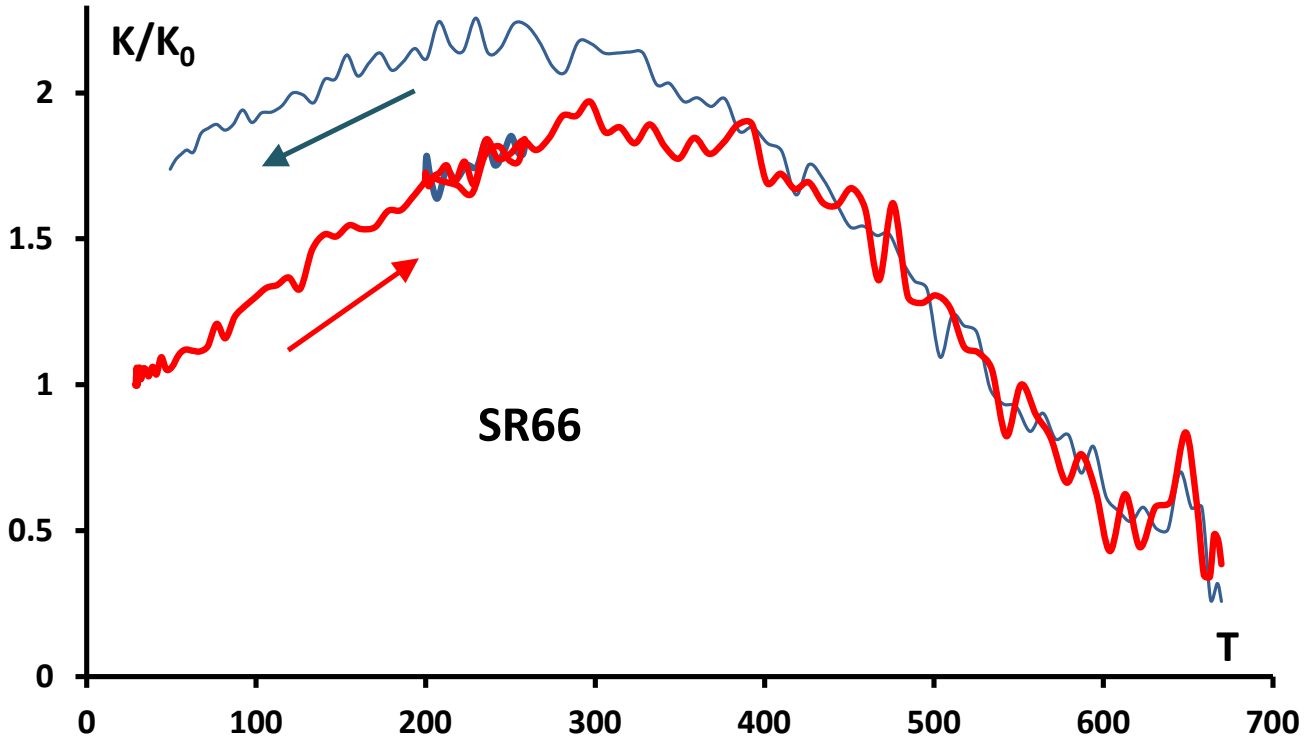
K/K0
2
1.5
1
0.5
0
SR66
T
0
100
200
300
400
500
600
700

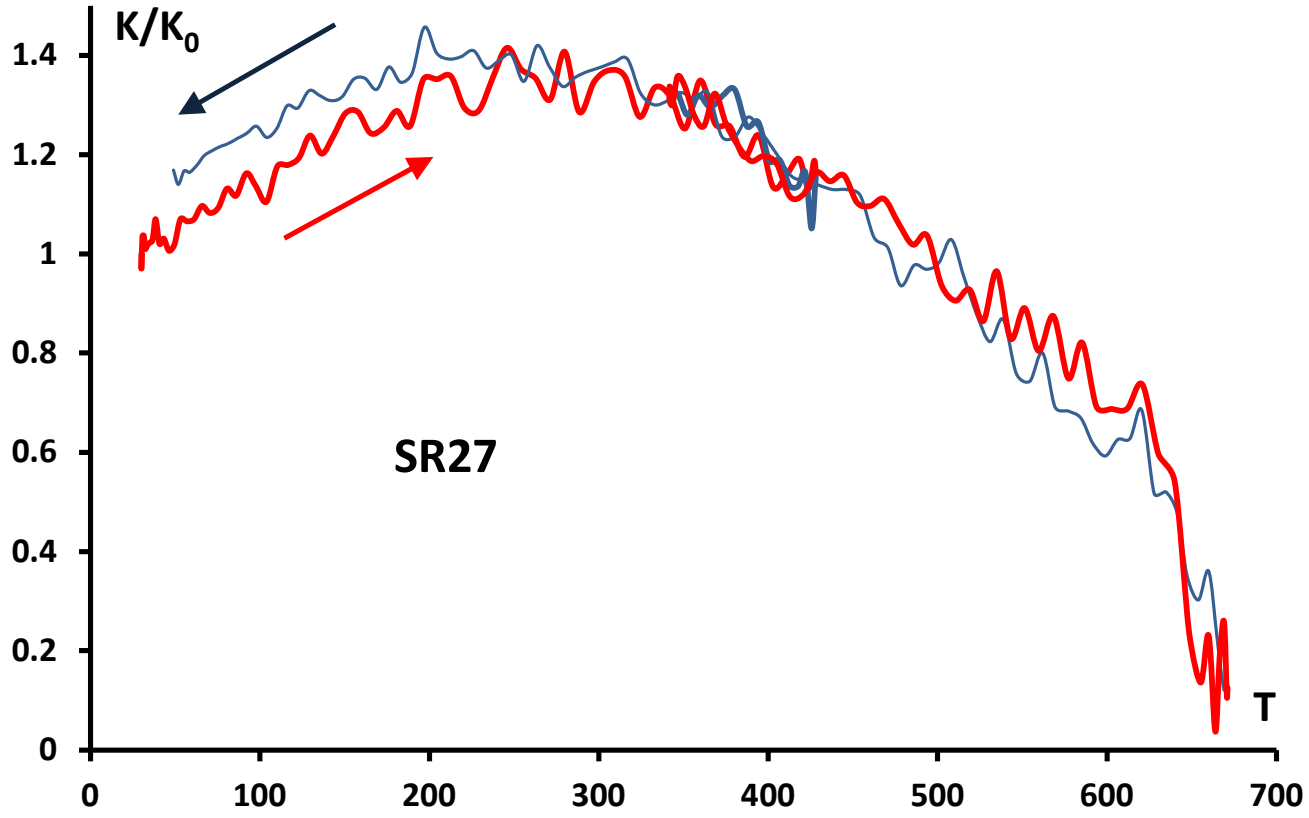
K/K0
1.4
1.2
1
0.8
0.6
0.4
0.2
0
SR27
T
0
100
200
300
400
500
600
700

Figure 9

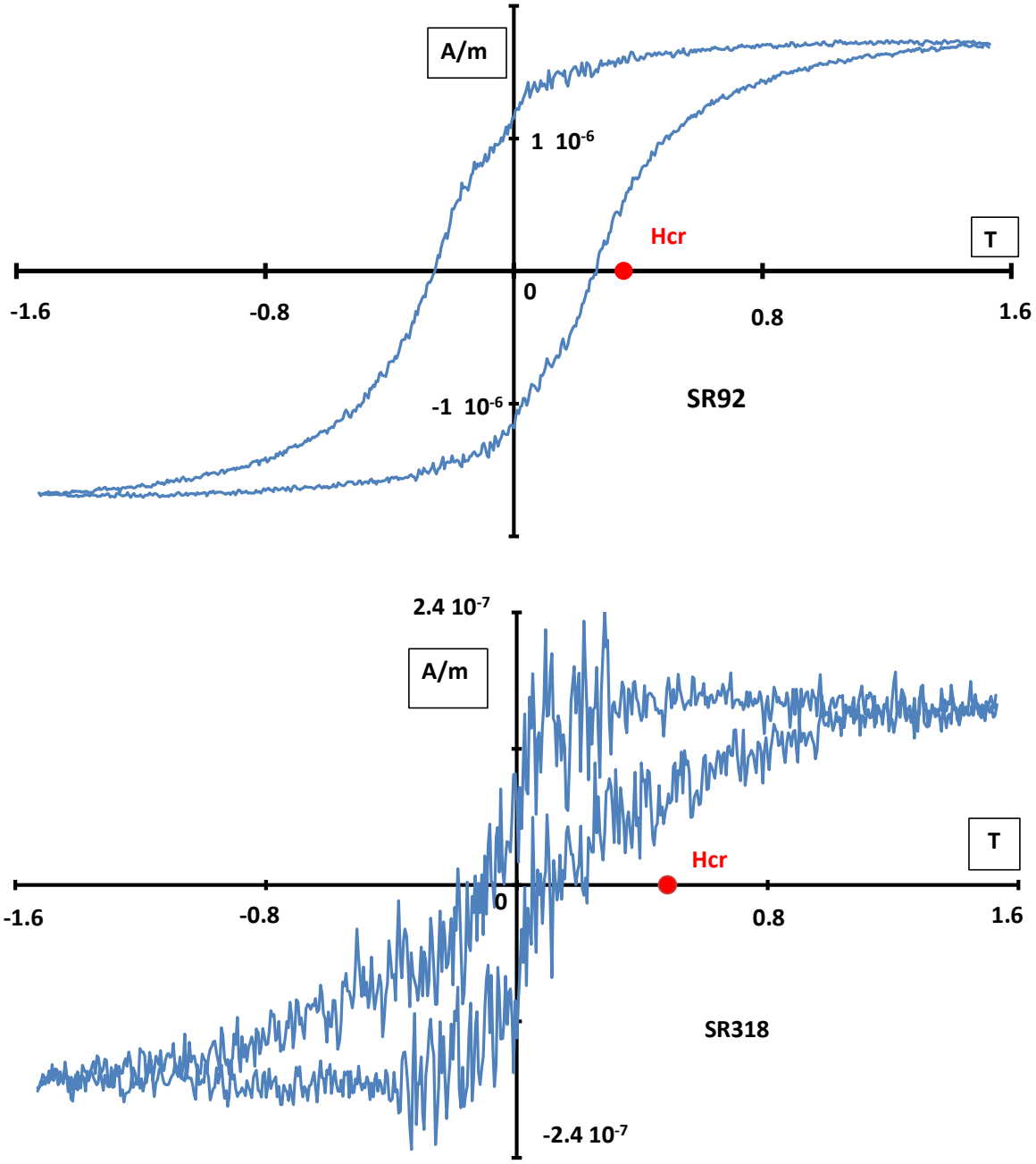
A/m
1 10-6
Hcr
T
-1.6
-0.8
0
0.8
1.6
-1 10-6
SR92
2.4 10-7
A/m
T
Hcr
-1.6
-0.8
0
0.8
1.6
SR318
-2.4 10-7

Figure 10

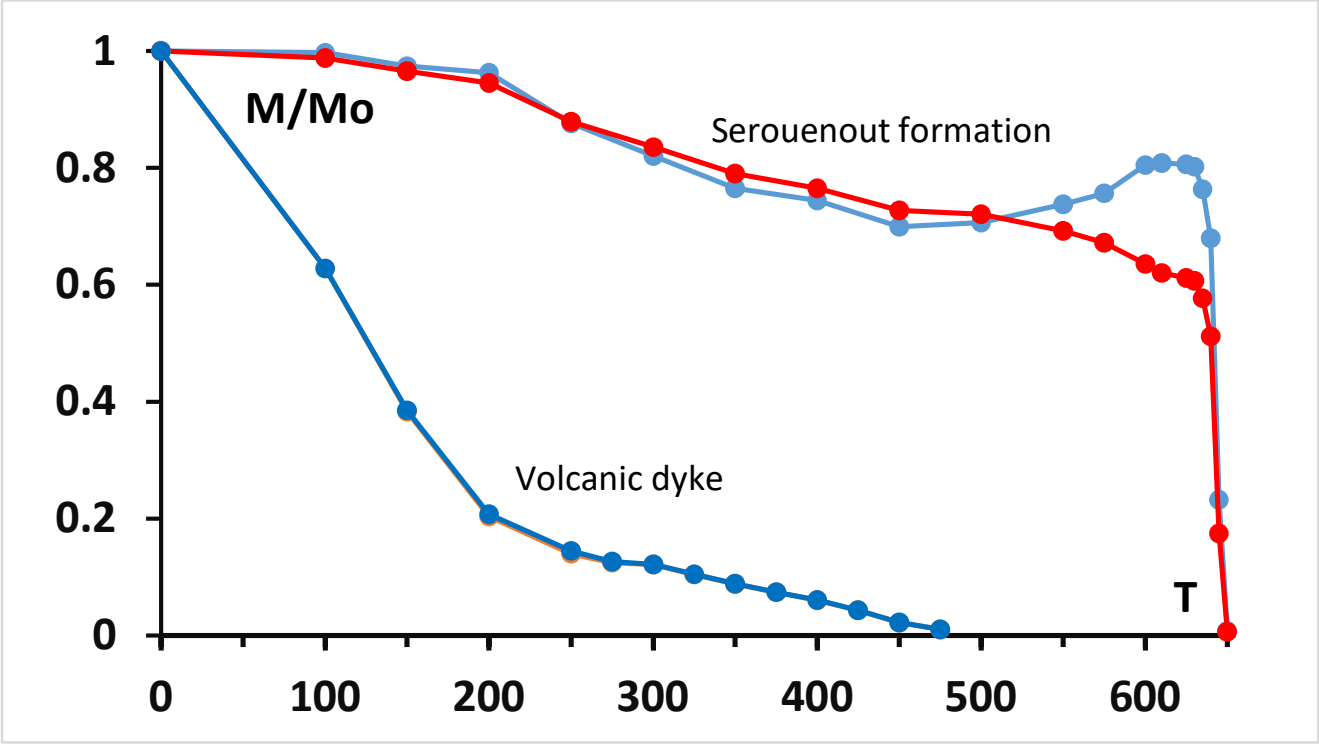
1
0.8
0.6
0.4
0.2
0
M/Mo
Serouenout formation
Volcanic dyke
T
0
100
200
300
400
500
600

Figure 11

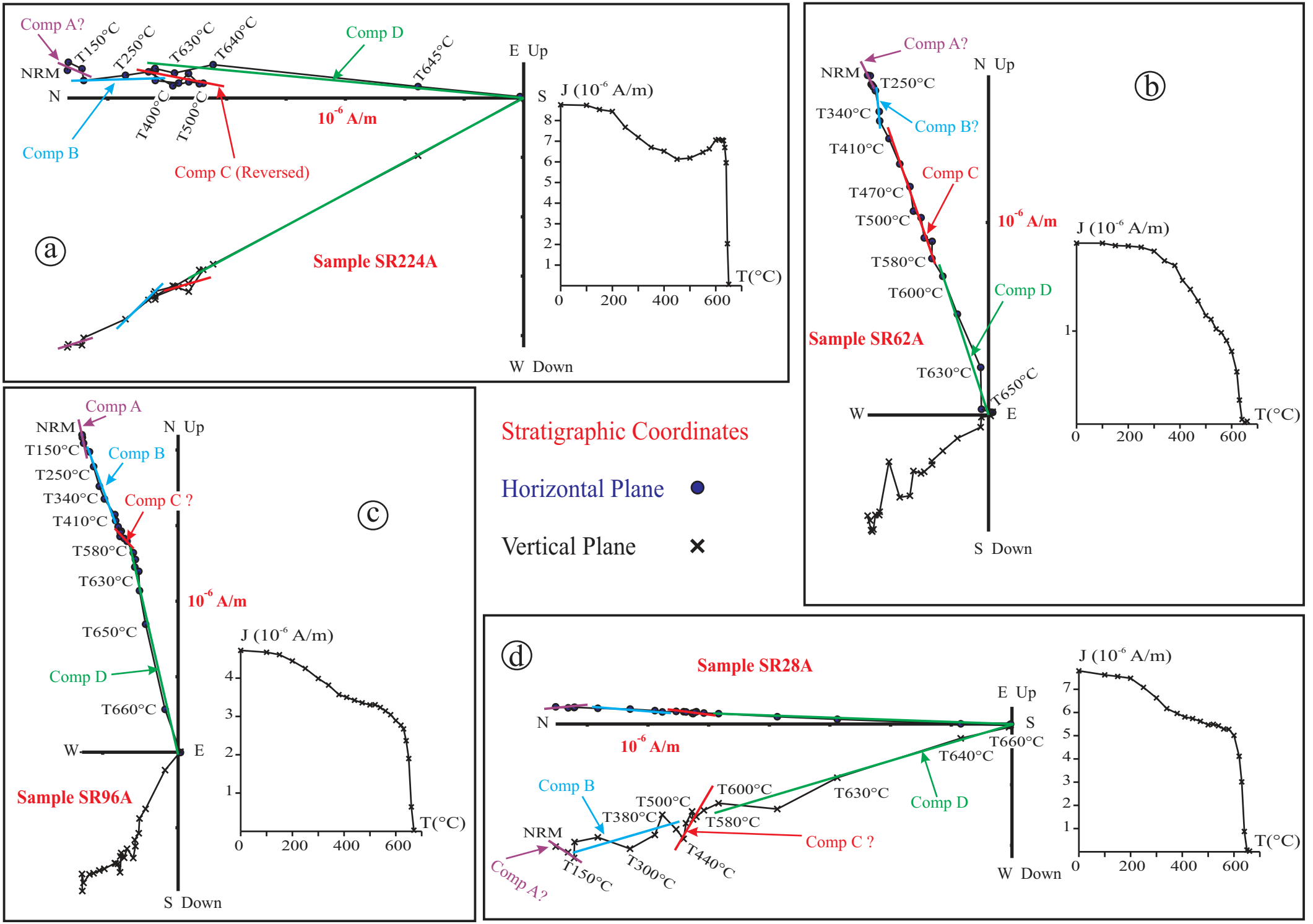
Comp A?
NRM
T150°C
T250°C
T630°C
T640°C
Comp D
T645°C
N
T400°C
T500°C
10^-6 A/m
Comp B
Comp C (Reversed)
E Up
S
J (10^-6 A/m)
8
7
6
5
4
3
2
1
T(°C)
0
200
400
600
W Down
a
Sample SR224A
Comp A?
NRM
T250°C
N Up
b
T340°C
Comp B?
T410°C
Comp C
T470°C
T500°C
10^-6 A/m
T580°C
T600°C
Comp D
Sample SR62A
T630°C
T650°C
W
E
J (10^-6 A/m)
1
T(°C)
0
200
400
600
S Down
Comp A
NRM
N Up
T150°C
Comp B
T250°C
T340°C
Comp C ?
T410°C
c
T580°C
T630°C
10^-6 A/m
T650°C
Comp D
T660°C
W
E
Sample SR96A
J (10^-6 A/m)
4
3
2
1
T(°C)
0
200
400
600
S Down
Stratigraphic Coordinates
Horizontal Plane
Vertical Plane
d
Sample SR28A
E Up
N
S
10^-6 A/m
T660°C
T640°C
Comp B
T500°C
T600°C
T630°C
Comp D
T380°C
T580°C
NRM
Comp C ?
T440°C
T150°C
T300°C
Comp A?
W Down
J (10^-6 A/m)
7
6
5
4
3
2
1
T(°C)
0
200
400
600

Figure 12

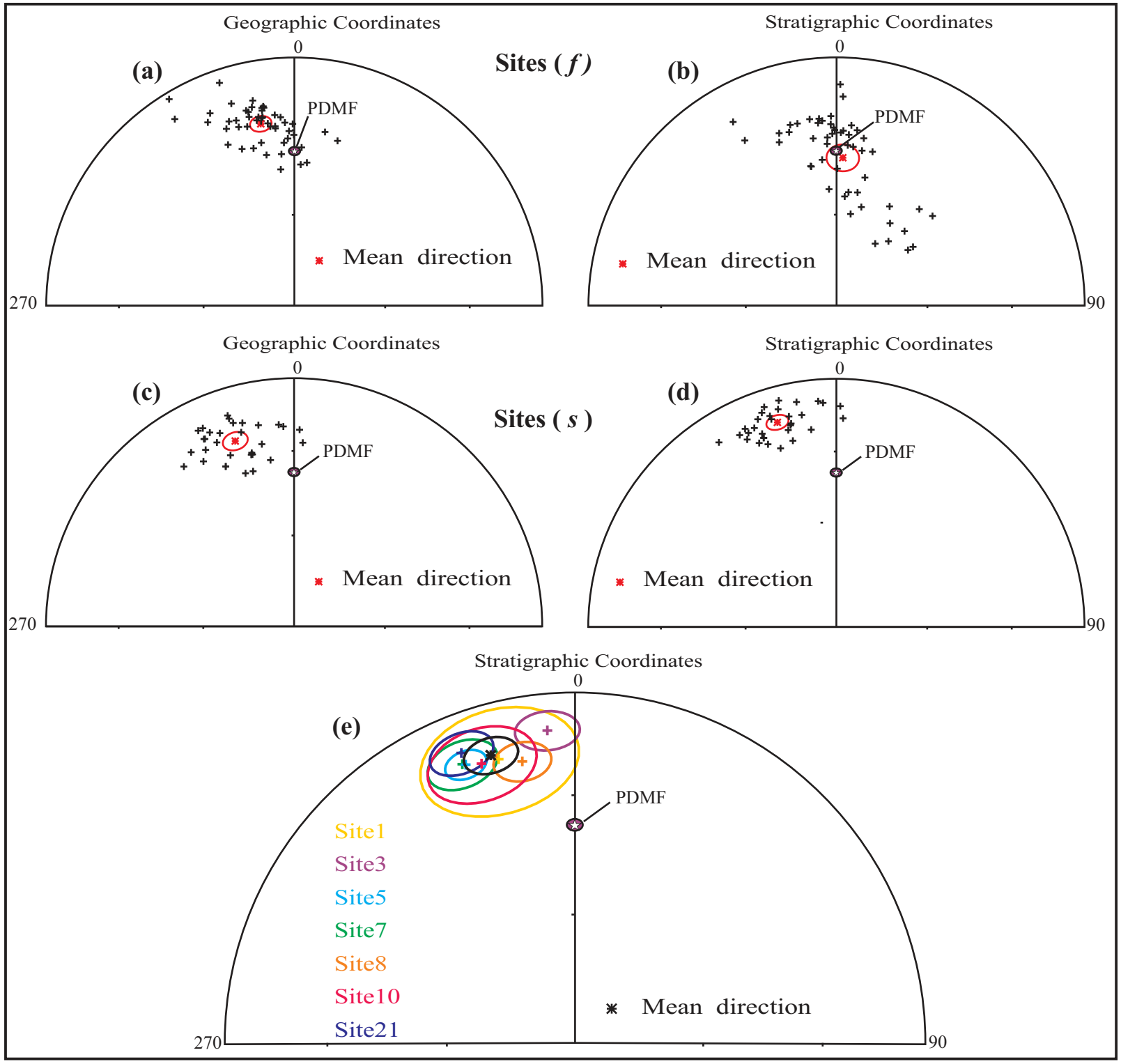
Geographic Coordinates
0
(a)
Sites (f)
PDMF
Mean direction
270
Stratigraphic Coordinates
0
(b)
PDMF
Mean direction
90
Geographic Coordinates
0
(c)
Sites (s)
PDMF
Mean direction
270
Stratigraphic Coordinates
0
(d)
PDMF
Mean direction
90
Stratigraphic Coordinates
0
(e)
PDMF
Site1
Site3
Site5
Site7
Site8
Site10
Site21
Mean direction
270
90

Figure 13

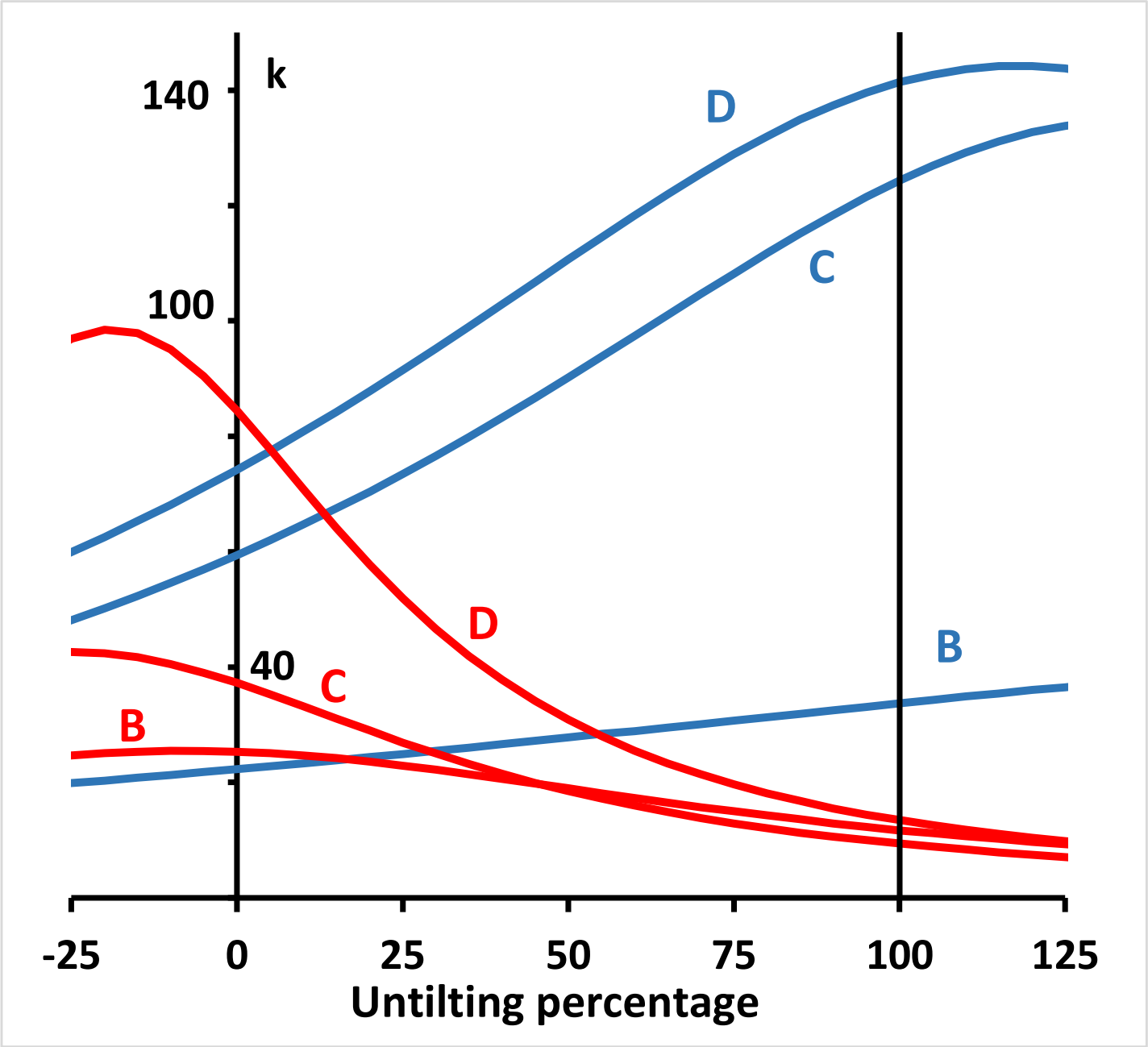

Figure 14

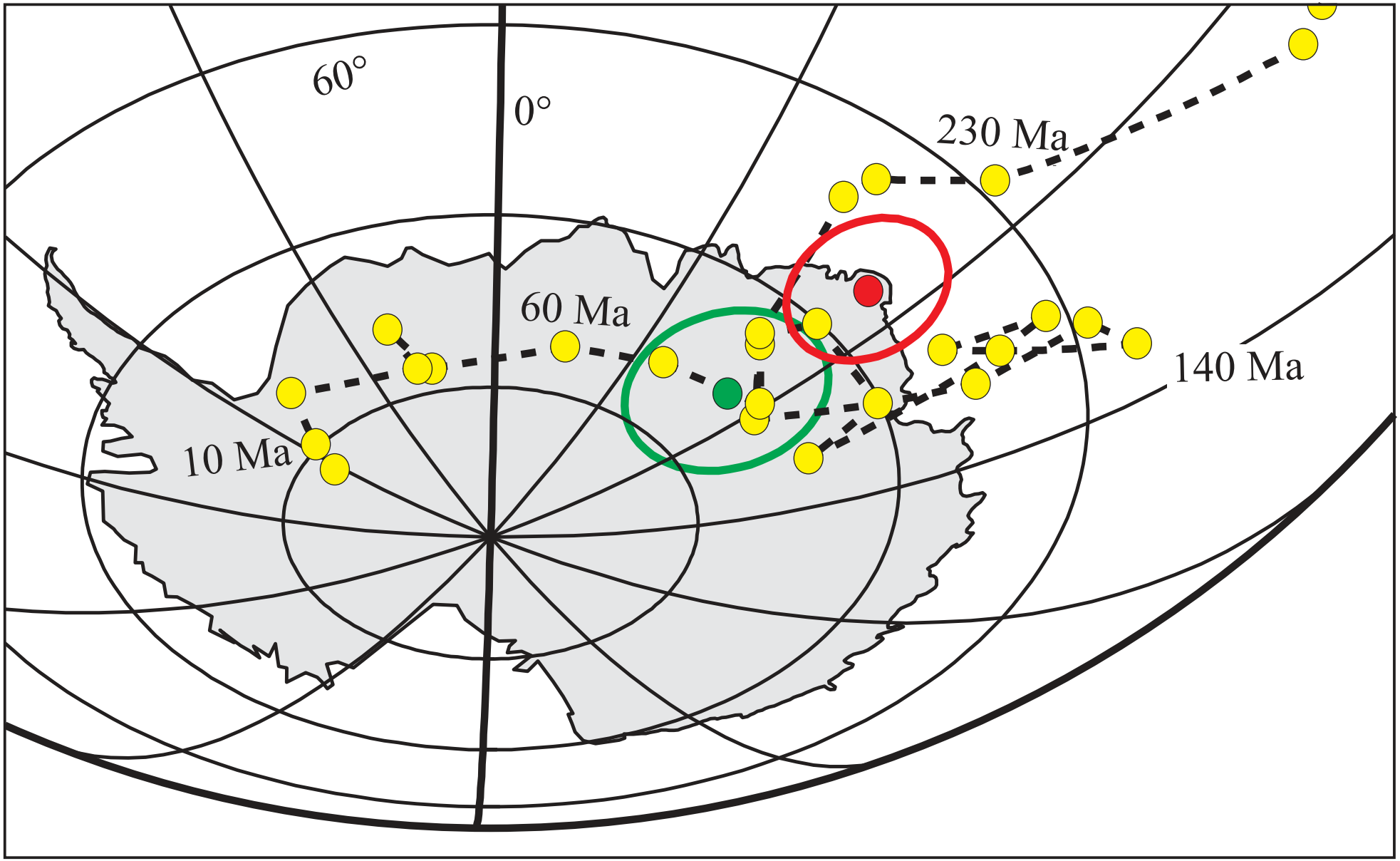

Figure 15

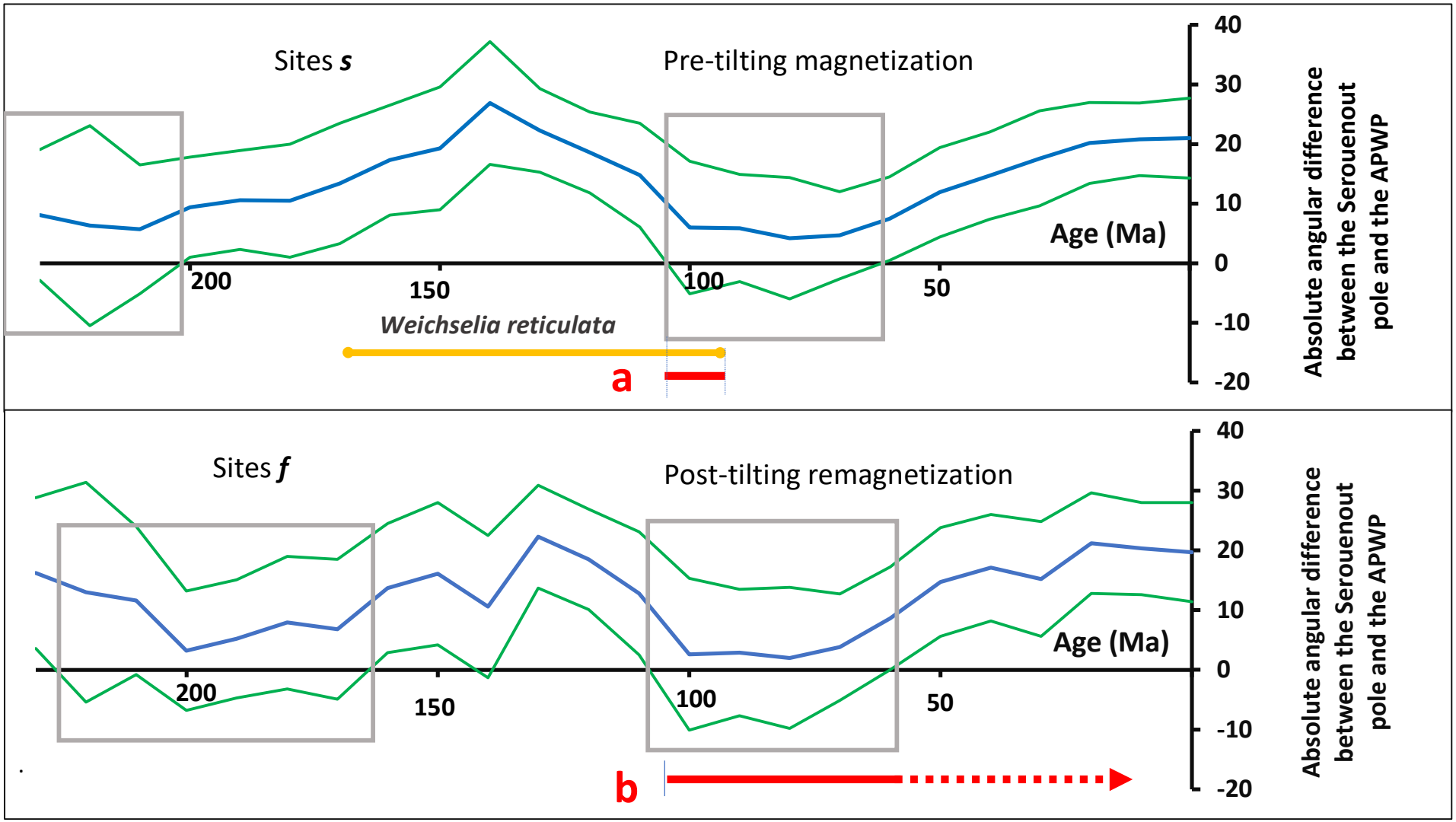
Sites *s*
Pre-tilting magnetization
Age (Ma)
200
150
100
50
40
30
20
10
0
-10
-20
Absolute angular difference between the Serouenout pole and the APWP
Weichselia reticulata
a
Sites *f*
Post-tilting remagnetization
Age (Ma)
200
150
100
50
40
30
20
10
0
-10
-20
Absolute angular difference between the Serouenout pole and the APWP
b

Table 1

site	P(°)	G(°)	comp	N	Dg(°)	Ig(°)	Ds(°)	Is(°)	k	α_{95}(°)
site 1	10	345	A	3	9.6	46.0	6.1	36.7	76	14.2
			B	4	323.1	43.8	325.9	34.4	4	52.9
			C	3	348.3	21.4	348.2	11.4	335	6.7
			D	3	344.9	27.2	344.9	17.2	67	15.1
Site 3	10	350	B	6	358.4	23.7	357.9	13.8	20	15.5
			C	4	357.6	33.1	356.9	23.2	43	14.2
			D	6	355.2	21.4	354.9	11.4	133	5.8
Site 5	0	0	B	6	336.8	9.1	336.8	9.1	20	14.4
			C	6	340.9	17.4	340.9	17.4	123	6.1
			D	6	338.5	15.7	338.5	15.7	284	4.0
Site 7	12	0	A	5	36.7	46.2	30.7	35.4	6	34.6
			B	5	331.8	37.5	335.5	25.0	32	13.7
			C	5	347.3	29.2	348.4	15.7	50	10.9
			D	6	335.9	27.7	338.0	15.3	100	6.7
Site 8	12	0	A	3	1.5	28.8	1.4	16.9	67	15.1
			B	5	351.8	25.0	352.3	13.1	21	17.1
			C	5	347.9	30.0	349.0	18.3	24	15.9
			D	4	348.3	31.1	349.4	19.3	279	5.5
Site 10	15	70	A	4	343.2	24.7	349.8	23.0	10	30.5
			B	5	339.2	10.0	341.8	9.9	12	22.8
			C	4	332.7	12.5	336.2	13.9	11	28.7
			D	3	336.9	16.8	341.5	17.0	140	10.5
Site 13	8	180	Volc	13	185.2	-39.2	185.9	-47.1	21	9.2
Site 16	12	90	A	7	359.9	29.3	6.6	28.6	39	9.8
			B	8	340.0	25.1	345.8	28.6	44	8.4
			C	9	341.6	24.7	347.4	28.0	52	7.2
			D	6	344.3	25.0	350.1	27.7	197	4.8
Site 17	18	100	B	8	347.5	25.7	356.9	31.3	38	9.2
			D	7	352.3	24.6	1.2	28.7	323	3.4
Site 18	18	100	B	10	77.5	31.6	80.3	14.7	2	44.7
			C inv	4	96.8	-9.4	96.5	-27.4	52	12.9
			C	6	2.1	41.3	18.1	41.2	24	13.9
			D	5	350.4	33.9	3.3	38.0	73	9.0
Site 19	40	140	B	8	340.3	26.5	1.0	61.8	13	16.1
			C	8	347.3	23.9	9.1	56.4	26	11.1
			D	8	347.8	20.2	6.5	53.0	86	6.0
Site 20	40	140	A	8	33.7	58.6	91.1	48.4	9	19.6
			B	8	23.8	55.4	83.5	52.4	13	16.2
			C	9	3.0	46.5	59.6	61.6	47	7.6
			D	8	2.3	36.8	42.7	57.1	102	5.5
Site 21	20	50	A	3	359.5	46.1	11.0	31.7	26	24.8
			B	3	324.9	21.6	332.3	18.6	30	23.1
			C	3	336.4	22.8	343.1	16.0	42	12.9
			D	3	333.4	17.7	338.6	12.1	426	6.0
Site 23	15	60	A	8	340.7	57.2	359.3	49.7	13	15.8
			B	8	353.2	64.0	14.8	55.4	5	26.3
			D	4	16.6	43.9	24.2	32.3	10	30.8

Site 24	20	110	A	7	0.9	32.1	14.4	36.5	5	28.5
			B	7	356.2	36.8	12.3	42.4	4	34.1
			C	6	337.2	31.9	349.8	43.9	20	15.5
			D	7	349.8	27.6	1.2	36.0	86	6.5
Site 25	17	10	A	8	346.5	38.2	0.3	45.9	20	12.6
			B	8	340.8	23.4	348.4	33.4	32	10.0
			C	7	330.4	24.0	337.3	36.3	21	13.6
			D	8	341.14	18.24	347.11	28.26	41	8.8

Table 1.

	comp	N	D_g (°)	I_g (°)	k_g	α_{95g} (°)	λ (°S)	φ (°E)	D_s (°)	I_s (°)	k_s	α_{95}s(°)	λ (°S)	φ (°E)
Sites f	**B**	7	349.3	37.3	17	15.2	81.8	85.3	6.4	47.2	10	19.6	80.9	238.9
	C	5	342.9	30.6	34	13.3	72.8	74.1	357.5	48.2	12	23.5	83.5	190.5
	D	7	**352.4**	**28.4**	**35**	**10.3**	**75.3**	**51.3**	5.2	38.8	19	14.4	**85.7**	**340.8**
Sites s	**B**	7	338.5	25.0	22	13.2	66.7	73.5	340.7	18.0	34	10.5	66.0	61.7
	C	7	344.1	24.0	58	8.0	70.8	60.7	346.0	16.6	122	5.5	69.2	69.4
	D	7	341.8	22.7	73	7.1	68.7	64.5	**343.7**	**15.5**	**140**	**5.1**	**67.2**	**53.6**

Table 2